Nonconvex Sparse Poisson Intensity Reconstruction for Time-Dependent Bioluminescence Tomography

Lasith Adhikari, Arnold D. Kim, and Roummel F. Marcia
Department of Applied Mathematics, University of California, Merced,
Merced, CA 95343 USA

***Abstract*—This paper concerns time-dependent bioluminescence imaging under low-photon conditions. In this problem, one seeks to reconstruct sources of light contained within a tissue sample from noisy boundary measurements of scattered light. The main challenge in this problem lies in processing signals that are constrained by partial differential equations. In this paper, we propose a novel two-stage method to recover time-dependent bioluminescent sources from boundary measurements corrupted by Poisson noise. Numerical experiments demonstrate the effectiveness of the proposed approach.**

I. Introduction

In bioluminescence imaging one seeks to reconstruct sources of light contained within a tissue sample from boundary measurements of scattered light. This imaging modality provides valuable insight into *in vivo* cellular and molecular processes in small animals, for example [1]. For this imaging problem, measured signals are modeled by solutions of an initial-boundary value problem of a partial differential equation modeling the multiple scattering of light by tissues. Hence, the main challenge in this problem lies in processing signals that are constrained by partial differential equations.

For this problem, it is reasonable to assume a sparse distribution of sources. In that regard, there have been several recent results that have employed sparsity-promoting methods to solve this bioluminescence imaging problem, *e.g.* [2]–[7]. For all of those studies, the sources did not vary in time. In contrast, Unlu and Gulsen [8] identify the importance of considering a time-dependent source for these imaging problems.

Motivated by this study, we take on the problem of reconstructing time-dependent bioluminescent sources. In particular, we consider measurements with relatively low photon counts so that one must explicitly consider Poisson noise in the data. For that case, we employ the nonconvex Sparse Poisson Intensity Reconstruction ALgorithm (SPIRAL-ℓ_p) [9] to solve the nonconvex problem for the negative Poisson log-likelihood function. We show that this approach applied to the time-averaged data provides an effective method for reconstructing the spatial support of the bioluminescent sources. Upon determining these supports, we recover the characteristic time decay of each of the sources from the time-dependent data. We show using numerical simulations that this two-stage reconstruction method effectively solves this time-dependent bioluminescence problem.

The remainder of this paper is as follows. In Section II, we describe the forward model and inverse problem that make up this time-depdendent bioluminescence imaging problem. In Section III, we describe the details of our two-stage method to recover the sources from boundary measurements of scattered light corrupted by Poisson noise. We give results from numerical simulations demonstrating this method in Section IV. Section V gives our conclusions.

II. Problem Formulation

Consider the domain Ω with boundary $\partial\Omega$ composed of a uniform absorbing and scattering medium. We assume that the optical properties of this medium are known to reasonable precision. Contained within Ω are a sparse distribution of time-dependent sources. For the time-dependent bioluminescence imaging problem, we seek to recover the spatial locations of these sources as well as their characteristic time behavior. In what follows, we describe the forward model and then the corresponding inverse problem for this bioluminescence problem.

A. Forward model

We model light scattering and absorption in the medium using the diffusion approximation [10], [11]. Let $\phi(\mathbf{r},t)$ denote the optical fluence rate at position $\mathbf{r}$ at time t. It satisfies the diffusion equation,

$$\frac{1}{c}\frac{\partial\phi}{\partial t} - \kappa\nabla^2\phi + \mu_a\phi = S \quad \text{in } \Omega\times(0,T], \tag{1}$$

with κ denoting the diffusion coefficient, μ_a denoting the absorption coefficient, and S denoting the time-dependent bioluminescent sources contained in the medium. We solve (1) subject to initial condition

$$\phi(\mathbf{r},0) = 0 \quad \text{in } \Omega, \tag{2}$$

and boundary condition

$$\phi + 2\kappa\partial_n\phi = 0 \quad \text{on } \partial\Omega\times(0,T] \tag{3}$$

Here, $\partial_n\phi$ denotes the outward normal derivative of ϕ. Note that S provides the only source of light in this problem. Upon solution of the initial-boundary value problem consisisting of (1) subject to (2) and (3), we model measurements of scattered light leaving the boundary of the medium, $u(\mathbf{r},t)$, through evaluation of

$$u(\mathbf{r},t) = -\kappa\partial_n\phi = \frac{1}{2}\phi \quad \text{on } \partial\Omega\times(0,T]. \tag{4}$$

Note that we have substituted (3) into the first result of (4) to obtain the final result of (4).

Suppose we consider the time-averaged data defined as

$$\bar{u}(\mathbf{r}) = \frac{1}{2}\bar{\phi}(\mathbf{r}) = \frac{1}{2T}\int_0^T \phi(\mathbf{r},t)\mathrm{d}t \quad \text{on } \partial\Omega. \tag{5}$$

The steady-state optical fluence rate, $\bar{\phi}$, satisfies the steady-state diffusion equation

$$-\kappa\nabla^2\bar{\phi} + \mu_a\bar{\phi} = \bar{S} \quad \text{in } \Omega, \tag{6}$$

subject to the boundary condition

$$\bar{\phi} + 2\kappa\partial_n\bar{\phi} = 0 \quad \text{on } \partial\Omega. \tag{7}$$

We will make use of this boundary value problem consisting of (6) subject to (7) in the analysis that follows.

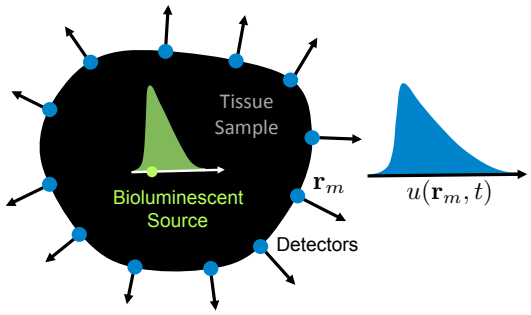

Fig. 1. Schematic diagram of time-dependent bioluminescence tomography. Photon-count measurements $u(\mathbf{r}_m, t)$ are collected at detectors, which are placed at boundary locations $\mathbf{r}_m$ for $m = 1, \ldots, M$.

B. Inverse problem

Suppose we take measurements of the scattered light leaving the boundary of the medium at M distinct locations denoted by $\mathbf{r}_m \in \partial\Omega$ for $m = 1, \cdots, M$. Moreover, suppose we collect N samples these measurements in time with sampling rate, Δt with $T = N\Delta t$. This entire collection of data is given by the vector $\mathbf{u} \in \mathbb{R}^{MN}$ with

$$\mathbf{u} = [u(\mathbf{r}_1, t_1), \cdots, u(\mathbf{r}_M, t_1), \cdots, u(\mathbf{r}_M, t_N)]. \tag{8}$$

Because these measurements have relatively low photon counts, these data are subject to Poisson noise.

The inverse problem seeks to reconstruct $S(\mathbf{r}, t)$ appearing in (1) from the set of noisy measurements in $\mathbf{u}$. Because the optical properties of the medium are assumed known, this inverse problem is a linear, inverse source problem. Nonetheless, it is severely ill-posed. We propose the following two-stage method for reconstructing the sources.

1) Assuming a sparse distribution of sources that does not change over $[0, T]$, we apply SPIRAL-ℓ_p, a nonconvex, sparsity promoting optimization method, to determine the spatial support of the sources from the time-averaged data (5).
2) Using the determined support of the sources from Step 1, we recover the characteristic time of decay for each of the sources.

In what follows, we give the details for this two-stage reconstruction method and then show results from numerical simulations to evaluate its effectiveness in solving this problem.

C. Related methods

Previous work for solving Poisson inverse problems include statistical multiscale modeling and analysis frameworks [12], nonparametric estimators using wavelet decompositions [13], and combination expectation-maximization algorithms with a total variation-based regularization [14]. Our proposed approach uses a sequence of separable approximations to the objective function with non-convex p-norm regularization to identify the support of the time-dependent bioluminescent sources and to recover their time decay.

III. Methodology

A. Finite difference discretization

We solve the initial-boundary value problem (1) subject to the initial condition (2) and the boundary condition (3) using the Crank-Nicolson method [15]. We discretize the spatial domain Ω with a 2D spatial grid of the form $x_i = i\Delta x$ and $y_j = j\Delta y$ for $i = 0, \ldots, N_x, j = 0, \ldots, N_y$. We also discretize the temporal domain $[0, T]$ into N equally spaced intervals of length Δt. We let the vector $\mathbf{V}^{\tilde{N}}$ have entries $(V^{\tilde{N}}_{0,0}, V^{\tilde{N}}_{1,0}, \ldots, V^{\tilde{N}}_{N_x-1,N_y-1})$, where $V^{\tilde{N}}_{i,j} \approx \phi(x_i, y_j, \tilde{N}\Delta t)$ and $1 \le \tilde{N} < N$. Similarly, we let the vector $\mathbf{S}^{\tilde{N}} = (S^{\tilde{N}}_{0,0}, S^{\tilde{N}}_{1,0}, \ldots, S^{\tilde{N}}_{N_x-1,N_y-1})$, where $S^{\tilde{N}}_{i,j} = S(x_i, y_j, \tilde{N}\Delta t)$. Then the Crank-Nicolson method leads to a linear model at time $\tilde{N}\Delta t$ in the form

$$\mathbf{L}^-\mathbf{V}^{\tilde{N}+1} - \mathbf{L}^+\mathbf{V}^{\tilde{N}} = \tilde{\mathbf{S}}^{\tilde{N}+1}, \tag{9}$$

where

$$\mathbf{L}^- = \left(1 + \frac{c\mu_a\Delta t}{2}\right)\mathbf{I} - \mathbf{L}_b,$$
$$\mathbf{L}^+ = \left(1 - \frac{c\mu_a\Delta t}{2}\right)\mathbf{I} + \mathbf{L}_b,$$

and

$$\tilde{\mathbf{S}}^{\tilde{N}+1} = (\mathbf{S}^{\tilde{N}+1} + \mathbf{S}^{\tilde{N}})\frac{c\Delta t}{2}.$$

Here, $\mathbf{L}_b$ is the $N_xN_y \times N_xN_y$ finite difference operator given by

$$\mathbf{L}_b\mathbf{V}^{\tilde{N}} = \frac{c\kappa\Delta t}{2\Delta x^2}(V^{\tilde{N}}_{i-1,j} - 2V^{\tilde{N}}_{i,j} + V^{\tilde{N}}_{i+1,j}) + \frac{c\kappa\Delta t}{2\Delta y^2}(V^{\tilde{N}}_{i,j-1} - 2V^{\tilde{N}}_{i,j} + V^{\tilde{N}}_{i,j+1}).$$

For all time levels, (9) can be written as a system of linear equations of the form

$$\underbrace{\begin{bmatrix} \mathbf{L}^- & 0 & \ldots & 0 \\ -\mathbf{L}^+ & \mathbf{L}^- & \ddots & \vdots \\ 0 & \ddots & \ddots & 0 \\ 0 & 0 & -\mathbf{L}^+ & \mathbf{L}^- \end{bmatrix}}_{\mathbf{L}} \underbrace{\begin{bmatrix} \mathbf{V}^1 \\ \mathbf{V}^2 \\ \vdots \\ \mathbf{V}^N \end{bmatrix}}_{\mathbf{V}} = \underbrace{\begin{bmatrix} \tilde{\mathbf{S}}^1 \\ \tilde{\mathbf{S}}^2 \\ \vdots \\ \tilde{\mathbf{S}}^N \end{bmatrix}}_{\tilde{\mathbf{S}}},$$

where $\mathbf{L}$ is a sparse lower triangular block matrix of size $NN_xN_y \times NN_xN_y$, containing $\mathbf{L}^-$ and $\mathbf{L}^+$. As defined in (4), in the discrete setting, time-dependent measurements are obtained by restricting the numerical solution $\mathbf{V}$ at the boundary:

$$\mathbf{u} = \frac{1}{2}\mathbf{R}\mathbf{V} = \frac{1}{2}\mathbf{R}\mathbf{L}^{-1}\tilde{\mathbf{S}},$$

where boundary restriction operator $\mathbf{R}$ is a sparse matrix of size $MN \times NN_xN_y$ and $\frac{1}{2}\mathbf{R}\mathbf{L}^{-1}$ is defined as the system matrix $\mathbf{A}$. Instead of generating the system matrix $\mathbf{A}$ explicitly, we compute the action $\mathbf{A}(\mathbf{x})$ and $\mathbf{A}^T(\mathbf{x})$ on-the-fly using the forward and backward substitution techniques. Similarly, the actions of time-independent system matrix also has to be constructed to solve the steady-state boundary value problem in (6) and (7). Next we describe a sparsity-promoting nonconvex optimization technique to recover interior sources.

B. Poisson intensity reconstruction

The arrival of photons at the detector is typically modeled by the Poisson noise model [16]:

$$\mathbf{y} \sim \text{Poisson}(\mathbf{A}\mathbf{f}^*),$$

where $\mathbf{y} \in \mathbb{Z}_+^m$ is a vector of observed photon counts, $\mathbf{f}^* \in \mathbb{R}_+^n$ is the vector of true signal intensity, and $\mathbf{A} \in \mathbb{R}_+^{m\times n}$ is the system matrix. Therefore, the Poisson reconstruction problem has the following constrained optimization form (see e.g., [17]):

$$\begin{aligned} \underset{\mathbf{f}\in\mathbb{R}^n}{\text{minimize}} \quad & \Phi(\mathbf{f}) \equiv F(\mathbf{f}) + \tau\ \text{pen}(\mathbf{f}) \\ \text{subject to} \quad & \mathbf{f} \succeq 0, \end{aligned} \tag{10}$$

where $F(\mathbf{f})$ is the negative Poisson log-likelihood function

$$F(\mathbf{f}) = \mathbf{1}^T\mathbf{A}\mathbf{f} - \sum_{i=1}^{m} y_i\ \log(\mathbf{e}_i^T\mathbf{A}\mathbf{f} + \beta),$$

where $\mathbf{1}$ is the m-vector of ones, $\mathbf{e}_i$ is the i-th column of the $m \times m$ identity matrix, $\beta > 0$ (typically $\beta \ll 1$), and pen: $\mathbb{R}^n \longrightarrow \mathbb{R}$ is a penalty functional. We solve (10) using the SPIRAL-ℓ_p approach proposed in [9], which we describe next.

C. SPIRAL-ℓ_p

Here, we consider $\text{pen}(\mathbf{f}) = \|\mathbf{f}\|_p^p$ $(0 \le p < 1)$ as the penalty function in (10). Then the generalized constrained optimization problem can be written as

$$\begin{aligned} \hat{\mathbf{f}} \quad = \quad & \underset{f\in\mathbb{R}^n}{\arg\min} \quad \Phi(\mathbf{f}) \equiv F(\mathbf{f}) + \tau\ \|\mathbf{f}\|_p^p \\ & \text{subject to} \quad \mathbf{f} \succeq 0, \end{aligned} \tag{11}$$

where $\tau > 0$. As described in [18], the solution of the problem (11) can be found by minimizing a sequence of quadratic models to the function $F(\mathbf{f})$ approximated by second-order Taylor series expansion where the Hessian replaced by a scalar multiple of the identity matrix $\alpha_k\mathbf{I}$ with $\alpha_k > 0$ [19]–[21]. Simplifying the second-order approximation yields a sequence of subproblems of the form

$$\begin{aligned} \mathbf{f}^{k+1} \quad = \quad & \underset{\mathbf{f}\in\mathbb{R}^n}{\arg\min} \quad \frac{1}{2}\ \|\ \mathbf{f} - \mathbf{s}^k\ \|_2^2\ + \frac{\tau}{\alpha_k}\ \|\ \mathbf{f}\ \|_p^p \\ & \text{subject to} \quad \mathbf{f} \succeq 0, \end{aligned} \tag{12}$$

where $\mathbf{s}^k = \mathbf{f}^k - \frac{1}{\alpha_k}\nabla F(\mathbf{f}^k)$. Note that the subproblem (12) can be separated into scalar minimization problems of the form

$$\begin{aligned} f^* \quad = \quad & \underset{f\in\mathbb{R}}{\arg\min} \quad \Omega(f) = \frac{1}{2}(f-s)^2 + \lambda|f|^p, \\ & \text{subject to} \quad f \ge 0. \end{aligned} \tag{13}$$

where f and s denote elements of the vectors $\mathbf{f}$ and $\mathbf{s}^k$ respectively and $\lambda = \tau/\alpha_k$. Given a regularization parameter $\lambda > 0$ and p-norm for $\Omega_s(f)$ in (13), there exists a threshold value $\gamma_p(\lambda)$ (that explicitly depends on p and λ) such that if $s \le \gamma_p(\lambda)$, the global minimum of (13) is $f_s^* = 0$; otherwise, the global minimum will be a non-zero value. When $s = \gamma_p(\lambda)$, there exists f_γ^* such that

$$\Omega_\gamma(f_\gamma^*) \ = \ \Omega_\gamma(0) \quad \text{and} \quad \Omega'_\gamma(f_\gamma^*) \ = \ 0. \tag{14}$$

By solving (14) simultaneously, we can explicitly find the threshold value $\gamma_p(\lambda)$ for given p and λ values. Specifically, $\gamma_p(\lambda)$ is given by $\gamma_p(\lambda) = (2\lambda(1-p))^{\frac{1}{2-p}} + \lambda p(2\lambda(1-p))^{\frac{p-1}{2-p}}$ (see [22] for details). For any $s > \gamma_p(\lambda)$, the unique minimum f_s^* of $\Omega_s(f)$ is greater than 0 and is obtained by setting Ω'_s to 0:

$$\Omega'_s(f_s^*) = f_s^* - s + \lambda p(f_s^*)^{p-1} = 0. \tag{15}$$

Details of the analysis of zero-finding algorithms to compute the root f_s^* can be found in [23].

D. Computational details

As we explained in Section II-B, our proposed method consists of two steps. In Step 1, we set the time-averaged measurements $\bar{\mathbf{u}}$ as the observation vector $\mathbf{y}$ of SPIRAL-ℓ_p algorithm, i.e., $\mathbf{y} = \bar{\mathbf{u}}$, while in Step 2, we set $\mathbf{y} = \mathbf{u}$. Similarly, the true signal $\mathbf{f}^*$ of SPIRAL-ℓ_p is set to the time-averaged $\tilde{\mathbf{S}}$ in Step 1, while $\mathbf{f}^*$ is $\tilde{\mathbf{S}}$ in Step 2. Note that the relevant system matrix also needs to be defined similarly according to each step.

IV. Numerical Results

In this section, we apply the proposed two-stage method for two 2D bioluminescence tomography problems. For the MATLAB simulations, we used the following optical properties: the absorption coefficient $\mu_a = 0.02$ and the diffusion coefficient $\kappa = 0.22$ [24]. We set $\Omega = (0,1) \times (0,1)$. Although this domain is considered to be small for the physical problem, it is sufficient to test and evaluate the method presented here. For both experiments, $N_x = N_y = 21$ and collected $N = 1000$ samples from $M = 72$ boundary detectors with sampling rate $\Delta t = 0.01$. Also, the decay rate of sources are set to 1.5. The simulated boundary measurements are corrupted by Poisson noise using the MATLAB's `poissrnd` function. The noise

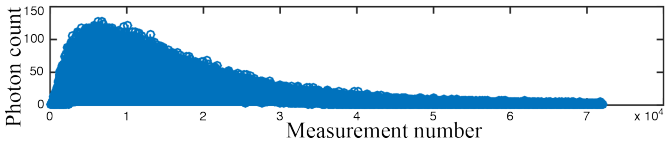

Fig. 2. Time-dependent measurements $\mathbf{u}$ corrupted by 15% Poisson noise.

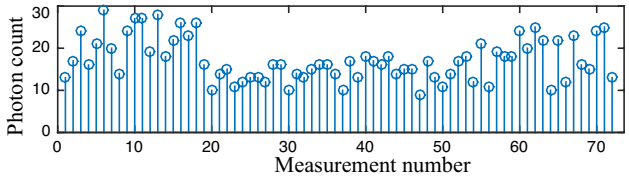

Fig. 3. Time-averaged measurements $\bar{\mathbf{u}}$ at the 72 boundary detectors.

level (%) is computed as $100 \cdot \|\mathbf{A}\mathbf{f}^* - \mathbf{y}\|_2 / \|\mathbf{y}\|_2$. The SPIRAL-$\ell_p$ algorithm is initialized using $\mathbf{A}^T\mathbf{y}$ and terminates if the relative difference between consecutive iterates converged to $\|\mathbf{f}^{k+1} - \mathbf{f}^k\|_2 / \|\mathbf{f}^k\|_2 \leq 10^{-8}$. The regularization parameters (τ) for both experiments are manually optimized to get the minimum RMSE (RMSE $(\%) = 100 \cdot \|\hat{\mathbf{f}} - \mathbf{f}^*\|_2 / \|\mathbf{f}^*\|_2$).

We are unaware of any other methods for solving time-dependent photon-limited bioluminescence problems, and thus, we do not present any comparisons with other methods.

A. Experiment 1

In this experiment, we wish to recover two bioluminescent point sources contained in the medium from approximately 15% Poisson noise corrupted time-dependent boundary measurements (see Fig. 2).

In the first step of our proposed method, we obtained the time-averaged measurements $\bar{\mathbf{u}}$ (see Fig. 3) and recovered the two locations accurately by solving the steady-state inverse problem using the SPIRAL-ℓ_p algorithm (see Fig. 4). Using the identified support in Fig. 4(b) and the time-dependent boundary measurements $\mathbf{u}$ in Fig. 2, we approximated the bioluminescent source intensities in space-time (see Fig. 5) by solving the time-dependent inverse problem using the SPIRAL-ℓ_1 approach. Specifically, since we have already identified the support for this intensity reconstruction, we use the ℓ_1-penalized SPIRAL without regularization (i.e., we set $\tau < \varepsilon$, where ε is machine precision) to reconstruct $\tilde{\mathbf{S}}$.

The decay rate for two point sources is computed by plotting the maximum intensity reconstruction of each time step in Fig. 5(b) over the time in semi-log scale (see Fig. 6). In particular, the decay rate is approximated by the negative reciprocal of the slope of the linear fit (represented by the orange line in Fig. 6) to the reconstruction (represented in red). In this experiment, the decay rate is approximately 1.54, while the true rate is 1.5.

B. Experiment 2

In this experiment, we wish to recover the support and the decay rate of two islands of pixels (see Fig. 7(a)) using 5% Poisson noise corrupted time-dependent measurements. By following the same approach as explained in Experiment 1,

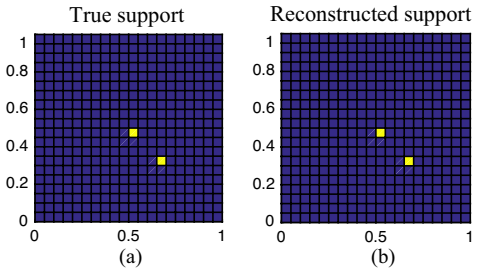

Fig. 4. Spatial support of the point sources from the time-averaged data in Fig. 3. (a) True locations of the sources, (b) SPIRAL-$\ell_p(p = 0.5)$ reconstructed support. Note the SPIRAL-ℓ_p method recovered the true support accurately.

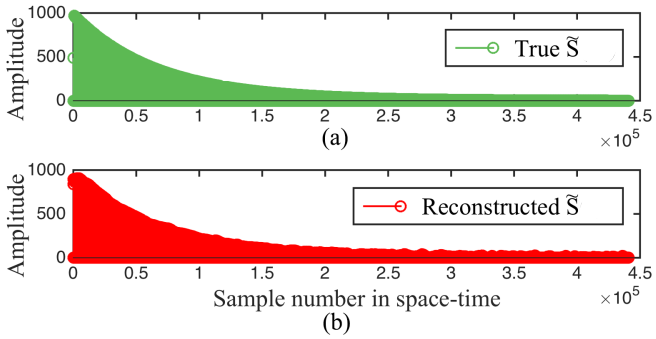

Fig. 5. (a) The true source intensities in space-time, (b) Reconstructed source intensities in space-time with RMSE = 5.63%. RMSE $(\%) = 100 \cdot \|\hat{\mathbf{f}} - \mathbf{f}^*\|_2 / \|\mathbf{f}^*\|_2$.

SPIRAL-ℓ_p identified the support of the sources (see Fig. 7(b)) with one spurious location (see the red box in Fig. 7(b)). To identify the support more accurately, we lowered the value of p from Experiment 1 to $p = 0.3$.

We used the recovered support (including the spurious location in Fig. 7(b)) to approximate the decay rate of the group of sources. Using a linear fit to the log of the intensity reconstruction (see Fig. 8), we estimated the decay rate to be

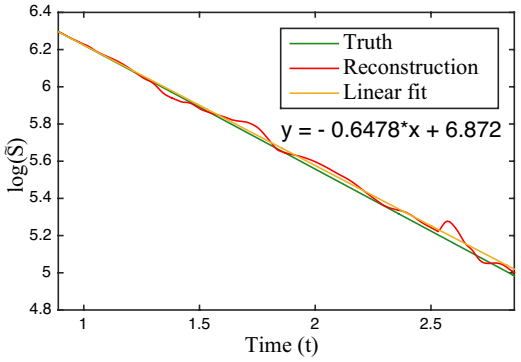

Fig. 6. Approximation of the decay rate of the two point sources. The estimated decay rate using a linear fit to the reconstruction is 1.54, while the true decay rate is 1.50. The decay rate is equal to the negative reciprocal of the slope of the curve in semi-log scale and the half-life period from the peak time-dependent measurement is used as the time window.

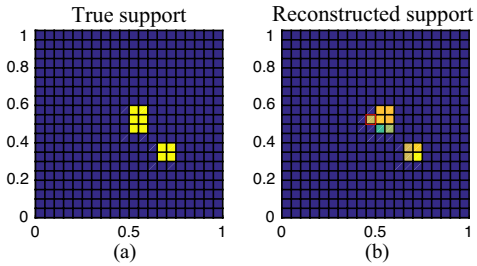

Fig. 7. Spatial support of the two group of sources from the time-averaged data. (a) True locations of the sources, (b) SPIRAL-$\ell_p(p = 0.3)$ reconstructed support. Note that there is a spurious support in the reconstruction which is marked by red color box.

1.53, while the true decay rate is 1.50.

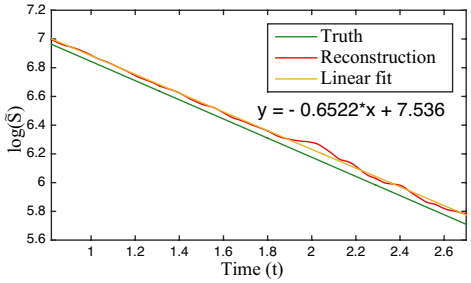

Fig. 8. Decay rate of the two group of interior sources. Approximated decay rate through a linear fit to the reconstruction is 1.53, while the true decay rate is 1.50. The decay rate is equal to the negative reciprocal of the slope of the curve in semi-log scale and the half-life period from the peak time-dependent measurement is used as the time window.

V. Conclusion

In this paper, we proposed a novel two-stage method to recover time-dependent bioluminescent sources from Poisson noise corrupted boundary measurements. Unlike previous methods, the first stage of our approach uses a nonconvex sparse Poisson intensity reconstruction method (SPIRAL-ℓ_p) to recover the support of the bioluminescent sources using the time-averaged data. In the second stage, we use the determined support of the sources to recover the characteristic time decay using the time-dependent data. Numerical experiments show that the proposed two-stage reconstruction method accurately solves this time-dependent bioluminescence problem. Furthermore, while this approach is efficient for small scale problems, it can be parallelized for large-scale problems.

Acknowledgment

This work was supported by National Science Foundation Grant CMMI-1333326. Lasith Adhikari's research is supported by the UC Merced Graduate Student Opportunity Fellowship Program.

References

[1] J. Feng, C. Qin, K. Jia, S. Zhu, X. Yang, and J. Tian, "Bioluminescence tomography imaging in vivo: recent advances," *Selected Topics in Quantum Electronics, IEEE Journal of*, vol. 18, no. 4, pp. 1394–1402, 2012.

[2] H. Gao and H. Zhao, "Multilevel bioluminescence tomography based on radiative transfer equation part 1: l1 regularization," *Optics Express*, vol. 18, no. 3, pp. 1854–1871, 2010.

[3] ——, "Multilevel bioluminescence tomography based on radiative transfer equation part 2: total variation and l1 data fidelity," *Optics Express*, vol. 18, no. 3, pp. 2894–2912, 2010.

[4] X. He, J. Liang, X. Wang, J. Yu, X. Qu, X. Wang, Y. Hou, D. Chen, F. Liu, and J. Tian, "Sparse reconstruction for quantitative bioluminescence tomography based on the incomplete variables truncated conjugate gradient method," *Optics Express*, vol. 18, no. 24, pp. 24 825–24 841, 2010.

[5] H. R. A. Basevi, K. M. Tichauer, F. Leblond, H. Dehghani, J. A. Guggenheim, R. W. Holt, and I. B. Styles, "Compressive sensing based reconstruction in bioluminescence tomography improves image resolution and robustness to noise," *Biomedical optics express*, vol. 3, no. 9, pp. 2131–2141, 2012.

[6] J. Feng, C. Qin, K. Jia, S. Zhu, K. Liu, D. Han, X. Yang, Q. Gao, and J. Tian, "Total variation regularization for bioluminescence tomography with the split bregman method," *Applied Optics*, vol. 51, no. 19, pp. 4501–4512, 2012.

[7] X. Zhang, Y. Lu, and T. Chan, "A novel sparsity reconstruction method from poisson data for 3d bioluminescence tomography," *Journal of scientific computing*, vol. 50, no. 3, pp. 519–535, 2012.

[8] M. B. Unlu and G. Gulsen, "Effects of the time dependence of a bioluminescent source on the tomographic reconstruction," *Applied Optics*, vol. 47, no. 6, pp. 799–806, 2008.

[9] L. Adhikari and R. F. Marcia, "Nonconvex relaxation for poisson intensity reconstruction," in *2015 IEEE International Conference on Acoustics, Speech and Signal Processing (ICASSP)*, April 2015, pp. 1483–1487.

[10] L. V. Wang and H.-i. Wu, *Biomedical Optics: Principles and Imaging*. John Wiley & Sons, 2012.

[11] S. R. Arridge, "Optical tomography in medical imaging," *Inverse Problems*, vol. 15, no. 2, p. R41, 1999.

[12] R. D. Nowak and E. D. Kolaczyk, "A statistical multiscale framework for poisson inverse problems," *IEEE Transactions on Information Theory*, vol. 46, no. 5, pp. 1811–1825, Aug 2000.

[13] A. Antoniadis and J. Bigot, "Poisson inverse problems," *The Annals of Statistics*, pp. 2132–2158, 2006.

[14] A. Sawatzky, C. Brune, T. Kösters, F. Wübbeling, and M. Burger, "EM-TV methods for inverse problems with Poisson noise," in *Level Set and PDE Based Reconstruction Methods in Imaging*. Springer, 2013, pp. 71–142.

[15] R. LeVeque, *Finite Difference Methods for Ordinary and Partial Differential Equations: Steady-State and Time-Dependent Problems*, classics in applied mathematics ed. SIAM, Society for Industrial and Applied Mathematics, 7 2007.

[16] D. L. Snyder and M. I. Miller, "Random point processes in space and time," *Springer-Verlag, New York, NY*, 1991.

[17] J. A. Fessler and A. O. Hero, "Penalized maximum-likelihood image reconstruction using space-alternating generalized em algorithms," *IEEE Trans. Image Processing*, vol. 4, no. 10, pp. 1417–1429, 1995.

[18] Z. T. Harmany, R. F. Marcia, and R. M. Willett, "This is SPIRAL-TAP: Sparse Poisson intensity reconstruction algorithms - theory and practice," *IEEE Trans. Image Processing*, vol. 21, no. 3, pp. 1084–1096, 2012.

[19] J. Barzilai and J. M. Borwein, "Two-point step size gradient methods," *IMA J. Numer. Anal.*, vol. 8, no. 1, pp. 141–148, 1988.

[20] E. G. Birgin, J. M. Martínez, and M. Raydan, "Nonmonotone spectral projected gradient methods on convex sets," *SIAM Journal on Optimization*, vol. 10, no. 4, pp. 1196–1211, 2000.

[21] S. J. Wright, R. D. Nowak, and M. A. T. Figueiredo, "Sparse reconstruction by separable approximation," *IEEE Trans. Signal Processing*, vol. 57, no. 7, pp. 2479–2493, 2009.

[22] W. Zuo, D. Meng, L. Zhang, X. Feng, and D. Zhang, "A generalized iterated shrinkage algorithm for non-convex sparse coding," in *2013 IEEE International Conf. on Computer Vision*, Dec 2013, pp. 217–224.

[23] A. Orkusyan, L. Adhikari, J. Valenzuela, and R. F. Marcia, "Analysis of p-norm regularized subproblem minimization for sparse photon-limited image recovery," in *2016 IEEE International Conference on Acoustics, Speech and Signal Processing (ICASSP)*, March 2016.

[24] J. C. Baritaux and M. Unser, "A primal-dual reconstruction algorithm for fluorescence and bioluminescence tomography," in *2011 IEEE International Symposium on Biomedical Imaging: From Nano to Macro*, 2011, pp. 960–963.